Hindawi
IET Electrical Systems in Transportation
Volume 2023, Article ID 9593445, 15 pages
https://doi.org/10.1049/2023/9593445

Research Article

Development of Wind-Powered Smart Transition Electric Vehicle Charging Station

Soumya Mohanty,[1] **Swagat Pati**,[1] **Sanjeeb Kumar Kar**,[1] **Aymen Flah**,[2,3,4,5] **Claude Ziad El-Bayeh**,[6] **and A. S. Veerendra**[7]

[1]*Department of Electrical Engineering, ITER, Siksha 'O' Anusandhan Deemed to be University, Bhubaneswar, India*
[2]*Processes, Energy, Environment and Electrical Systems, National Engineering School of Gabes, University of Gabes, Gabes 6072, Tunisia*
[3]*MEU Research Unit, Middle East University, Amman, Jordan*
[4]*College of Engineering, University of Business and Technology (UBT), Jeddah 21448, Saudi Arabia*
[5]*The Private Higher School of Applied Sciences and Technology of Gabes, University of Gabes, Gabes, Tunisia*
[6]*Department of Electrical Engineering, Bayeh Institute, Amchit, Lebanon*
[7]*Department of Electrical and Electronics Engineering, Manipal Institute of Technology, Manipal Academy of Higher Education, Manipal 576104, India*

Correspondence should be addressed to Swagat Pati; swagatpati@soa.ac.in and A. S. Veerendra; veerendra.babu@manipal.edu

Received 14 June 2023; Revised 27 July 2023; Accepted 22 August 2023; Published 27 November 2023

Academic Editor: Ayman Al-Quraan

The power industry is embracing green energy solutions to meet growing demand along with advancement in its technological innovations. Among the myriad innovations, electric spring stands out as a cutting-edge technology, embracing the concept of smart load to intelligently manage power systems. Concurrently, the emergence of electric vehicles (EVs) has paved the way for a new branch of power networks in the transport system. Ingeniously combining these two trends, a smart charging mechanism has been developed through an EV charging station within an isolated microgrid having a wind energy conversion system as the lone and primary source. To ensure optimal performance and stability, a sophisticated smoothening band charge controller has been developed. This controller enables seamless transitions between fast and slow charging modes, effectively curbing noncritical voltage fluctuations beyond permissible thresholds. In order to demonstrate the superior efficacy of the smoothening band charge controller, a comprehensive comparative study was conducted, analyzing its performance against rapid transition controllers. The results highlight the remarkable advantages of the smoothening band approach, further solidifying its significance in future smart charging systems. To validate the proposed system, rigorous testing was carried out using the state-of-the-art OPAL-RT 4510 real-time simulator. The successful validation marks a pivotal step toward the widespread adoption of this innovative and environmentally conscious approach in the power industry.

1. Introduction

Islands and remote communities encounter challenges in electrical power generation due to their isolated geographical locations [1]. Traditionally, they heavily rely on diesel generators, leading to environmental and logistical problems along with high greenhouse gas emissions. The transportation of diesel to these isolated areas also poses risks. Therefore, the ongoing power system era is eventually shifting its focus toward renewable energy resources to develop a base for the next-generation electricity market, which must be sustainable and nature-friendly [2]. Moreover, global researchers and industrialists are constantly gearing up to make the transportation system an integral part of the electricity network because conventional transportation systems heavily depend upon fossil fuel resources. In the beneath of the aforementioned facts, electric vehicles (EVs) are gaining importance as one of the most prominent business opportunities for the next few decades [3]. While analyzing the load structure of an islanded system, it is observed that islands do not have heavy

industrial loads, resulting in higher total electricity demand during the evening compared to the daytime. Additionally, EV charging loads are often higher in the evening. Therefore, wind energy could be a much preferable option over solar energy in this context due to the unavailability of solar incidence in peak time. Further, from the core electrical control perspective, the association of renewable energy sources and EVs with the existing power system is challenging in various ways. A few of the challenges are uncertain variations of power, voltage, and frequency [4–6], harmonics distortion [7], severe impact on microgrids at peak hours [8], etc. On top of that, the exponentially increasing vehicle count driven by electricity can bring a sudden spike in the electrical market in the form of EV charging stations. This major change can certainly affect the everlasting peak demand issue because most EVs undergo uncontrolled charging [9, 10]. To address the increased load resulting from a substantial number of EVs on the existing distribution system, specific active measures need to be implemented. To tackle this issue, there are a number of research works have been suggested. In the study of Yoon and Kang [11], the EV charging work is confined to residential microgrids where the challenges are much lesser in comparison to an islanded grid. A nonlinear program is solved in the study of Shaaban et al. [12] for ensuring the optimum operation cost of EV charging is proposed, but they obtained a compromising solution to satisfy the joint objective. In the study of Clairand et al. [13], an EV aggregator communicates with the system operator to manage charging and respect grid constraints. The primary drawback of this approach is the substantial excess energy generated by RES, which cannot be fully utilized by EVs despite having high-RES capacity installation. Wang et al. [14] demonstrate the benefits of coordinated charging with reactive power support, reducing average EV charging costs. Another solution for this problem is wireless sensor network deployment in power systems to optimize energy management [15–17], which can be a tedious job for an islanded system. Apart from these, much research has also been conducted for vehicle-to-grid operations to ensure proper demand side management (DSM) [18–20], but that requires a fast charger. However, fast chargers are mostly designed with unidirectional Vienna rectifiers for cost reduction [21]. Hence, there is a research gap to make sure both DSM and EV charging facilities should coexist in an islanded environment that can operate efficiently.

A novel smart load (SL) solution called electric spring (ES) can provide cutting-edge technology to overcome voltage-frequency instabilities as per some of the recently published studies [22–27]. Several studies have been carried out for scaling up the abilities of ES and presented in various research articles [28–31]. Moreover, according to the implementation perspective, several generations of ES have been reported in these articles. While generation one of ES (ES-G1) [32] is the capacitor-based source that only has the capability of reactive power transfer and control. The ES-G2 [33] simply replaces the capacitor part with a battery to add in the active power control. The subsequent generation, i.e., ES-G3 has come up with an enhanced operating range facility by replacing noncritical load (NCL) with a bidirectional converter-battery arrangement, contrasting the ES fundamental concept [34]. Further innovations are presented eventually, such as back-to-back converter-based ES (B2BES) [35], PV-fed ES [36, 37], AC/DC converted-based ES (ACDCES) [38], coordinated power-controlled ES [39], etc. The PVES is always subjected to the uncertainty of solar power, thus requiring high storage devices. On the other hand, the bidirectional ACDCES eliminates the DC/DC conversion system associated with both B2BES and PVES, thus restricting some power losses and costs. Going further, the coordinated power control properly manages power between nonlinear load and battery storage to optimize the size and capacity of the battery. Moreover, ES has already been utilized in a variety of applications and still proceeding in its footsteps toward new innovative implementations [40, 41]. In one of such implementations, ES is utilized in EV charging [42, 43] so as to maintain nominal voltage across the critical load (CL). However, the impact of EV charging on noncritical loading is still uncovered. This scenario is even critical in islanded microgrid systems where surplus power support is always a hurdle, unlike grid-connected systems. This gap in research has been attempted to address in this work. In addition to that, the effect of EV charging becomes more severe when the system considered lacks inertia. Especially self-excited induction generator (SEIG)-based systems that work in the saturation region of the magnetization curve will be most adversely affected by EV charging. This motivated the authors to study the effect of EV charging with a low inertia SEIG system.

In this work, a 550 kVA SEIG-based isolated system is taken into consideration. The voltage stabilization of the system is done by an ES. The SEIG-ES system houses an EV charging station, which is part of the CL. The EV charging station is considered to be a combination of a diode rectifier and DC–DC buck converter, which gives a charging voltage of 48 V. Simple voltage control for the buck converter is utilized for controlling the charging current of the EV.

The major contribution of this work is as follows:

(i) The maiden application of the EV charging station in a much more challenging environment, such as a SEIG-based isolated system, is implemented where the system is prone to severe voltage and frequency variations.

(ii) ES has been employed to maintain the overall voltage of the islanded system, providing DSM technology.

(iii) In most of the literatures, ES is used as voltage regulator; emphasis is given on maintaining the voltage profile of the CL. This work, on the contrary, proposes a combined control strategy that not only enhances the CL voltage profile but also improves the NCL voltage profile by controlling the charging speed of the EV through a smoothening band charge control approach.

(iv) Moreover, in scenario where EVs are being charged or discharged, their power demands can cause fluctuations in the overall voltage. These voltage variations

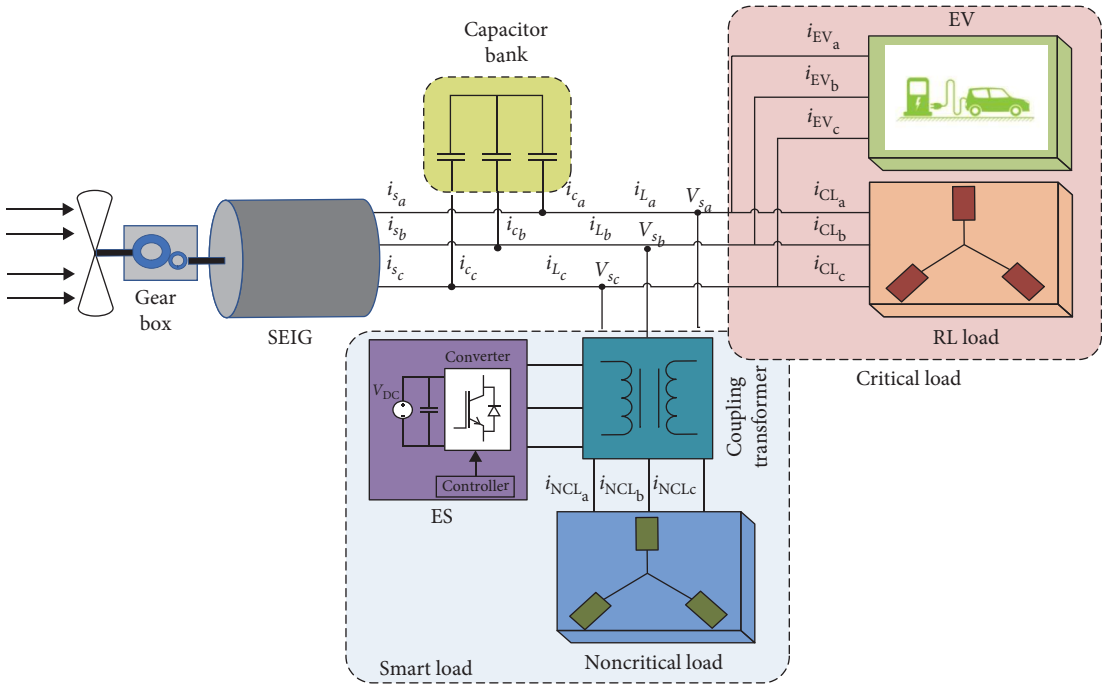

FIGURE 1: Remote islanded system diagram.

can potentially impact sensitive equipment or devices, which is also addressed in this study.

(v) Through simulation in MATLAB/Simulink is performed to understand the behavior of the system under different operating conditions, EV charging scenarios, and external factors. To further validate the accuracy and effectiveness of simulated results, the OPAL-RT 4510 platform is utilized. By running the simulation model on the OPAL-RT 4510, the complex power system behavior is replicated.

2. Test System Description

The test setup depicted in Figure 1 is the focus of this discussion. It is an independent system composed of a three-phase, 550 kVA SEIG with a capacitor bank connected in a delta configuration, along with both critical and NCLs, an injection transformer, and an ES. The SEIG functions as an islanded wind energy conversion system, while the ES comprises a bidirectional voltage-controlled voltage source converter, a DC link battery, and an AC side LC filter. Further information on the various components is provided in subsequent subsections. Table 1 provides the system specification.

2.1. SEIG Modeling. A self-excited induction machine is a type of squirrel-cage induction machine that can operate as a generator without the need for an external electrical power source. The self-excitation process in a SEIG is achieved through a capacitive bank connected to the stator terminals. In this research, the SEIG is depicted in the stationary reference frame, and the modeling equations for the SEIG are presented in the form of Equations (1)–(10).

$$V_{ds} = R_s i_{ds} + \frac{d}{dt}\psi_{ds}, \tag{1}$$

$$V_{qs} = R_s i_{qs} + \frac{d}{dt}\psi_{qs}, \tag{2}$$

$$V_{dr} = R_r i_{dr} + \frac{d}{dt}\psi_{dr} - \omega_r \psi_{qr}, \tag{3}$$

$$V_{qr} = R_r i_{qr} + \frac{d}{dt}\psi_{qr} + \omega_r \psi_{dr}. \tag{4}$$

The equation for the electromagnetic torque is as follows:

$$T_e = \frac{3}{2}\frac{P}{2} L_m \left(i_{qs} i_{dr} - i_{ds} i_{qr}\right). \tag{5}$$

The magnetizing inductance (L_m) of the SEIG is a function of magnetizing current (I_m), I_m is given as follows:

$$I_m = \frac{\sqrt{\left(i_{ds} + i_{dr}\right)^2 + \left(i_{qs} + i_{qr}\right)^2}}{\sqrt{2}}. \tag{6}$$

The provided equations below represent the terminal voltages.

$$\frac{dV_{as}}{dt} = \frac{\left(i_{ca} - i_{cb}\right)}{3C}, \tag{7}$$

$$\frac{dV_{bs}}{dt} = \frac{\left(2i_{ca} - i_{cb}\right)}{3C}, \tag{8}$$

Table 1: Specification of the test system.

Induction generator components	Values
Number of pole (P)	6
Magnetizing inductance (L_m)	0.0065 if $I_m \leq 8$ 0.0065–0.0003*(I_m−80) if $8 < I_m < 130$ 0.005–0.00001*(I_m−130) if $130 < I_m < 400$ 0.002156 if $I_m > 400$
Per phase leakage inductance of stator (L_s)/rotor (L_r)	0.1397 mH
Capacitance (C)	980 μF
Stator resistance (R_s)	0.05 Ω/phase
Rotor resistance (R_r)	0.049 Ω/phase
Inertia (J)	13.05 kg.m^2
Damping coefficient (B)	0.122 N/rad/s
Electric spring components	**Values**
Inverter topology	3Ø Voltage source converter
Switching frequency	5 kHz
Cutoff frequency	750 Hz
DC link voltage	250 V
Filter inductance	0.18 mH
Filter capacitance	250 μF

$$V_{ab} + V_{bc} + V_{ca} = 0, \tag{9}$$

where

$$\left.\begin{aligned} i_{ca} &= i_{ga} - i_{la} \\ i_{cb} &= i_{gb} - i_{lb} \\ i_{cc} &= i_{gc} - i_{lc} \end{aligned}\right\}. \tag{10}$$

2.2. ES Modelling. ES is a voltage source converter that creates a springing effect in the electrical system. However, the application of ES demands load categorization. There are two types of system loads: CL and NCL. An NCL is a load that can endure some degree of voltage instability. On the other hand, CL is the load that operates at a limited voltage range. When ES and NCL are arranged in series, the resulting configuration is called a SL, as illustrated in Figure 1. This technology works by varying the voltage across the NCL to maintain a steady voltage across the CL. The modeling equation of ES is given in Equations (11)–(15). The modulation index for the three phases is represented by MI_a, MI_b, and MI_c respectively.

$$\left.\begin{aligned} MI_a &= 2SW_a - 1 \\ MI_b &= 2SW_b - 1 \\ MI_c &= 2SW_c - 1 \end{aligned}\right\}, \tag{11}$$

where SW_a, SW_b, and SW_c are the switching states. These variables can take binary values, relying on the logic of switching.

The phase voltages of the voltage source converter can be represented as follows:

$$\left.\begin{aligned} V_{ia} &= \frac{V_{dc}}{2}\left(\frac{2}{3}MI_a - \frac{1}{3}MI_b - \frac{1}{3}MI_c\right) \\ V_{ib} &= \frac{V_{dc}}{2}\left(\frac{2}{3}MI_b - \frac{1}{3}MI_c - \frac{1}{3}MI_a\right) \\ V_{ic} &= \frac{V_{dc}}{2}\left(\frac{2}{3}MI_c - \frac{1}{3}MI_a - \frac{1}{3}MI_b\right) \end{aligned}\right\}, \tag{12}$$

where "V_{dc}" is the DC side voltage of the inverter.

The line–line potential difference can be as follows:

$$\left.\begin{aligned} V_{iab} &= V_{ia} - V_{ib} \\ V_{ibc} &= V_{ib} - V_{ic} \\ V_{ica} &= V_{ic} - V_{ia} \end{aligned}\right\}. \tag{13}$$

Harmonics elimination is ensured through an inductor–capacitor filter. The filter currents can be given as follows:

$$\left.\begin{aligned} \frac{d}{dt}i_{fa} &= \frac{1}{L_f}\left(V_{ca} - V_{ia} - R_f i_{fa}\right) \\ \frac{d}{dt}i_{fb} &= \frac{1}{L_f}\left(V_{cb} - V_{ib} - R_f i_{fb}\right) \\ \frac{d}{dt}i_{fc} &= \frac{1}{L_f}\left(V_{cc} - V_{ic} - R_f i_{fc}\right) \end{aligned}\right\}. \tag{14}$$

The voltage across the filter capacitor can be expressed as follows:

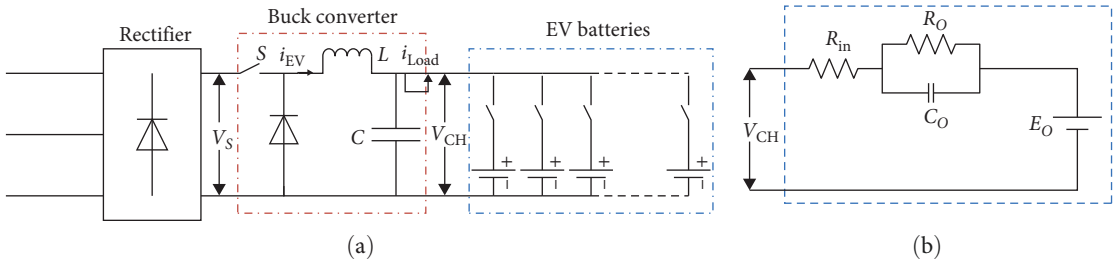

FIGURE 2: (a) Schematic diagram of electric vehicle. (b) Battery structure.

$$\left.\begin{aligned} V_{ca} &= \frac{1}{C_c}(i_{al} - i_{fa}) \\ V_{cb} &= \frac{1}{C_c}(i_{bl} - i_{fb}) \\ V_{cc} &= \frac{1}{C_c}(i_{cl} - i_{fc}) \end{aligned}\right\}. \tag{15}$$

To make the ES currents (i_{esa}, i_{esb}, i_{esc}) and the NCL currents (i_{al}, i_{bl}, i_{cl}) equal, the transformer ratio chosen to be 1 : 1.

2.3. Load Modeling. The studies system comprises two kinds of loads, those are NCL and CLs. The CL consists of two parts, i.e., a linear load and an EV charging station. The NCL is considered to be linear RL load.

2.3.1. Modeling of Linear Load. The linear loads used in the system are governed by Equations (16)–(18). All the loads are assumed to be three-phase balanced loads.

$$V_{as} = i_{as}R_{al} + L_{al}\frac{di_{as}}{dt}, \tag{16}$$

$$V_{bs} = i_{bs}R_{bl} + L_{bl}\frac{di_{bs}}{dt}, \tag{17}$$

$$V_{cs} = i_{cs}R_{cl} + L_{cl}\frac{di_{cs}}{dt}. \tag{18}$$

2.3.2. Modeling of Electric Vehicle Charging Station. In this work, the EV charging station is considered to be a rectifier that feeds a charge controller. The charge controller is considered in this work is a buck regulator which maintains the output voltage within a range of 48–52 V. The buck regulator dynamic equation is expressed in Equations (19) and (20).

$$\frac{di_L}{dt} = \frac{SV_s}{L} - \frac{V_O}{L}, \tag{19}$$

$$\frac{dV_O}{dt} = \frac{i_L}{C} - \frac{i_{Load}}{C}, \tag{20}$$

where i_L and V_O are the inductor current and output voltage of the buck converter as shown in Figure 2(a). "S" is the switching state of the switch, which can be either be "1" or "0".

As can be seen in Figure 2(a), the proposed EV charging station is capable for charging multiple EV simultaneously. The charging of EV in this proposed work is taken to be equivalent to the charging of the battery. The battery model considered in this work is given by the equation below.

The equivalent circuit for the EV battery considered in this work is given in Figure 2(b). The isolated system becomes vulnerable when EV is introduced in the system due to limitations in source power. So, the power controller becomes essential for balancing. Here, a DSM technology called ES is proposed.

3. System Design

The system under consideration is an isolated system with a 550 kVA SEIG as its main power generator. The NCL is rated for 350 kVA at a nominal voltage of 230 V. Taking a CL to NCL ratio of 0.45, and the CL kVA can be set as 160 kVA. In this work, the allowable range of operation for the NCL is taken to be 230–130 V rms. This gives an ES injection voltage range from 0 to 100 V. The ES injection voltage is zero when the NCL voltage is 230 V. As the ES injection voltage increases the power consumed by the ES increase. So, the kVA rating of the ES would be decided for the maximum value of injection voltage, i.e., 100 V.

The kVA of the NCL with a voltage value of 130 V can be calculated as follows:

$$\mathrm{NCL}_{\mathrm{kVA}_{130v}} = 3V_{ph} \times I_{ph} = 111.8\mathrm{kVA}. \tag{21}$$

So, NCL current at a voltage of 130 V will be as follows:

$$I = \frac{111.8 \times 10^3}{3 \times 130} = 286.6A. \tag{22}$$

For injecting a voltage of 100 V, the dc voltage requirement of the ES [44] would be given as follows:

$$V_{dc} > \frac{2\sqrt{2}V}{\sqrt{3}m_a}. \tag{23}$$

Considering a modulation index $m_a = 0.7$
We get $V_{dc} > 233V$

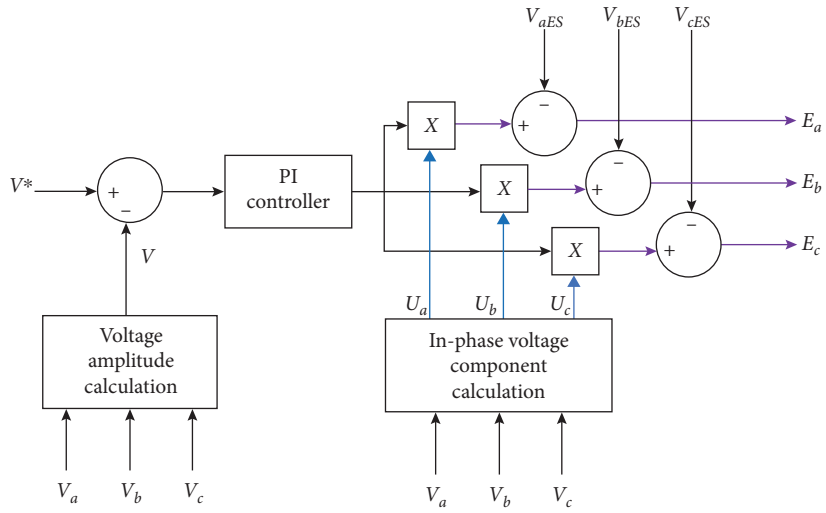

FIGURE 3: Minimum voltage control structure.

So, the authors have considered the value of V_{dc} to be 250 V.

For designing the LC filter values of the ES, the peak current value can be expressed as follows [45]:

$$I_{peak} = \frac{\sqrt{2}V}{2\varsigma_C}\sqrt{\frac{C_f}{L_f}}. \tag{24}$$

From this work a damping ratio of $\varsigma_c = 0.5$ is considered. Further from Kim et al. [45], the ratio of L_f/C_f can be limited by the expression given below:

$$\frac{L_f}{C_f} > \frac{V}{\sqrt{2}\varsigma_C I_{peak}} = \frac{250}{\sqrt{2}\times 0.5\times 404.4} > 0.8. \tag{25}$$

So, the value of L_f/C_f is considered as 0.85 in this work. Again, considering a cutoff frequency of 750 Hz.

We get

$$\sqrt{LC} = \frac{1}{W_e} = 0.00021, \tag{26}$$

which gives the filter inductance value to be $L_f = 0.18$ mH. The filter capacitance can be calculated as $C_f = 245\mu$ F $\approx 250\mu$ F.

4. Control of Electrical Spring (ES)

The control mechanism of ES is displayed in Figure 3. It further explains the determination of SEIG voltage amplitude (V_t) and in-phase components (u_a, u_b, u_c). These are calculated as per Equations (27) and (28).

$$V_t = \sqrt{\frac{2}{3}(V_a{}^2 + V_b{}^2 + V_c{}^2)}, \tag{27}$$

$$u_a = \frac{V_a}{V_t},\ u_b = \frac{V_b}{V_t},\ u_c = \frac{V_c}{V_t}. \tag{28}$$

The voltage amplitude (V_t) is further taken for the calculation of the error signal. The compensation voltage is generated from the PI controller, which takes the error signal as input. The product of compensation voltage along with the in-phase voltage components (u_a, u_b, u_c) are calculated in the next step. Further, the actual injected voltages are compared with the reference injected voltages and the output reference voltage errors (E_a, E_b, E_c) are injected into PWM to generate converter gate pulses. These operations enable ES to produce the required voltage.

4.1. Proposed Smoothing Band Control Strategy. In most of the literature where ES was implemented for the voltage regulation of the CL, efforts have been made to stabilize the CL voltage. The NCL voltage profile was mostly regulated by the previously set value of NCL to CL ratio. More the NCL to CL ratio smaller will be the voltage deviation across NCL, and more will be the range of operation of the ES. But getting a large NCL to CL ratio in an isolated system most of the time is not feasible in isolated systems. So, in this work, authors propose a smoothing band-based coordinated control structure for the system. The proposed scheme simultaneously takes care of the CL voltage without deteriorating the NCL voltage to extreme extents. The abundance of NCL composition enables wider range flexibility to maintain a constant CL voltage. An NCL-to-CL ratio of 9 : 1 has proven to be highly effective [46]. But it is always not possible to maintain such a ratio practically, and a low ratio may result in a highly deteriorated NCL voltage profile. Therefore, the effectiveness of the proposed control strategy with a lower NCL-to-CL ratio is demonstrated further. In this work, a low NCL to CL ratio of 2.22 : 1 is considered to show the effectiveness of the proposed control strategy. The proposed control strategy helps in improving the NCL voltage profile by adjusting the charging speed of the EV. The proposed

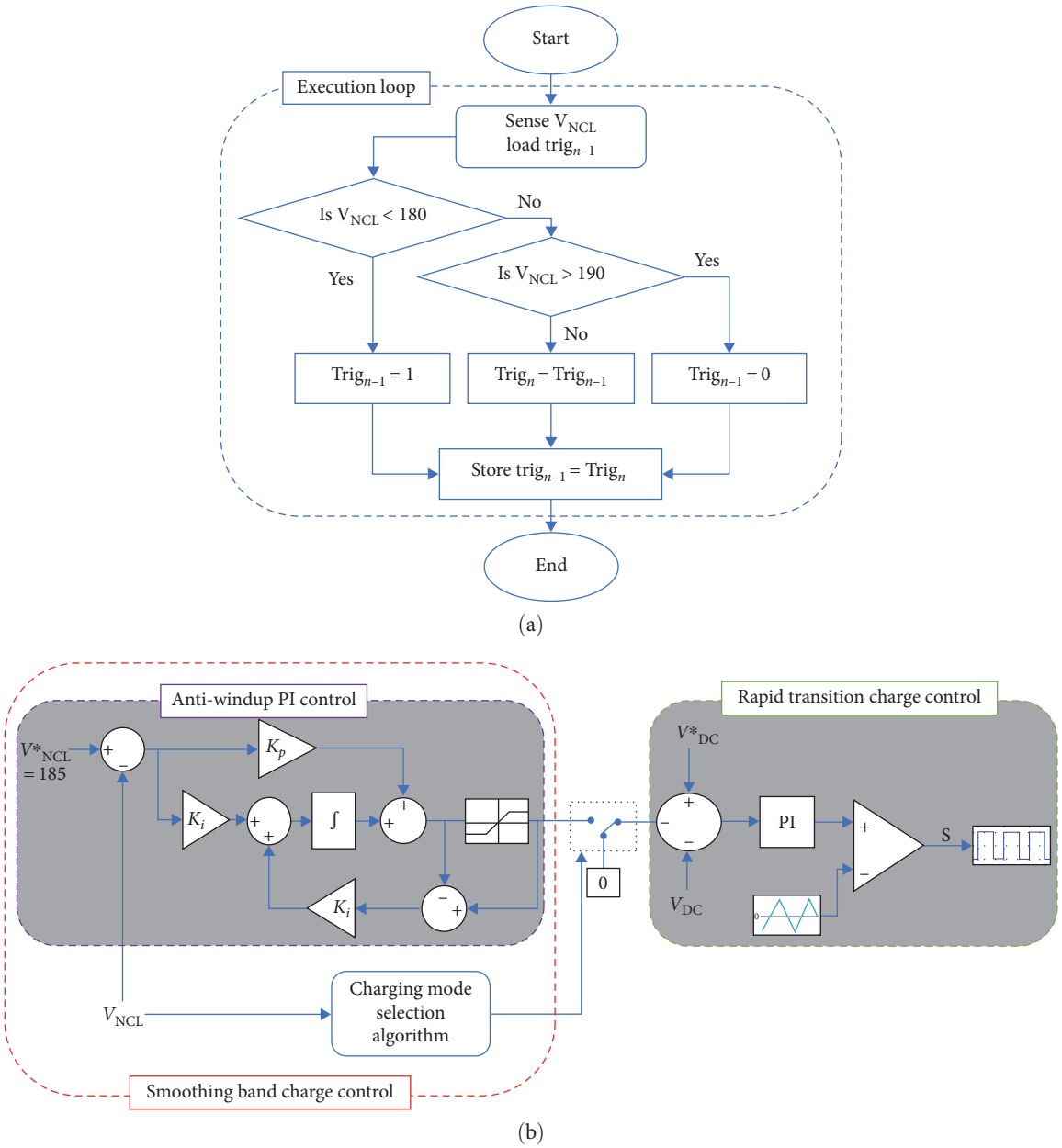

FIGURE 4: (a) Flowchart for smooth band control strategy. (b) Schematic diagram of proposed control strategy.

control structure is shown in Figure 4(a). A smoothing band is decided, which decides the mode of charging of the EV, taking the NCL voltage profile into consideration. The charging mode selection algorithm is shown in the flow chart as in Figure 4(a). The selection algorithm decides the trigger value to be enabled or disabled according to the NCL voltage value. If the NCL voltage falls below 150 V, the trigger signal is enabled, and the smoothing band control comes into operation. At this time, both the control schemes, the rapid charging control, and the smoothing band control, coordinately operate to maintain the EV charging at a slower pace, as can be seen in Figure 4(b). On the other hand, the ES control scheme at this time manages the CL voltage. As the system power demand reduces and the voltage starts rising, and the NCL voltage rises above 170 V, the selection algorithm disables the trigger signal. With the trigger signal disabled the smoothing band control again comes out of operation and the EV charging is totally controlled by only the rapid transition charge control scheme. The trigger signal can never be independent and always depends upon the NCL voltage value. The band of 20 V, which is from 150 to 170 V, provides a smooth transition between the charging modes and also avoids unnecessary switching between modes near the set voltage value.

As can be seen from the control structure of the charging station in Figure 4(b), as soon as the NCL voltage reduces below the minimum set value of 150 V, the trigger signal is enabled. Enabling the trigger signal results in external signal

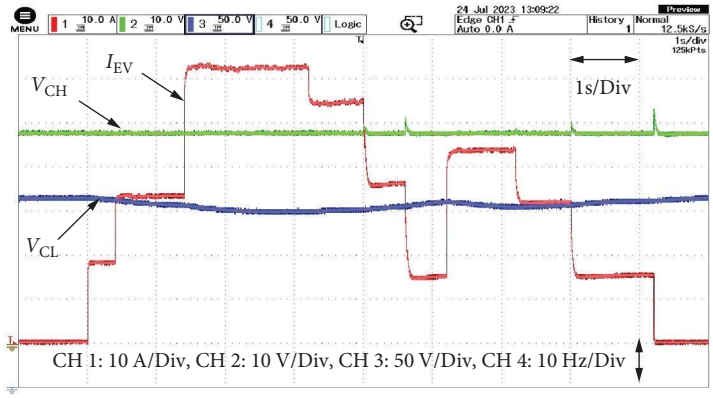

FIGURE 5: Charging of multiple vehicles without ES.

"ext" to be subtracted from the reference set voltage of the buck converter. The signal "ext" is generated from the NCL voltage control loop, as can be perceived in Figure 4(b). So, subtraction of the signal "ext" reduces the DC reference output voltage of the buck converter so as to reduce the charging current. Reduction in charging current helps in improving the NCL voltage. The PI controller used in the NCL voltage loop is a controller with an anti-windup mechanism, as shown in Figure 4(b). This anti-windup PI controller tries to keep the NCL voltage at a reference voltage of 155 V. As the generated power increases or the load is reduced the NCL voltage increases. When the NCL voltage increases above the upper limit of 170 V the trigger is disabled, and EV rapid charging is again enabled. The transition of charging mode is decided within the voltage band of 150–170 V.

5. Simulation and Result

In this section, the performance of the proposed control algorithm is evaluated and compared with that of the traditional charging of multiple EVs without ES and rapid transition charge control algorithm. The performances of the control algorithms are tested by subjecting the system to step variation in the charging current of the EV charging station. The charging current is varied from zero to a maximum of 120 A in several steps. During the whole work, the CL and NCL are taken to be at constant loading conditions. The SEIG torque is also considered to be constant during the whole work. In the first subsection, the performance of the rapid transition charge control is evaluated and analyzed. The second subsection shows the performance of the proposed smoothing band charge control. The third subsection shows the power quality aspects of the system with the proposed smoothing band charge control structure with FFT analysis and THD of different system currents and voltages.

5.1. Traditional Charging without ES. In a traditional charging setup, the EVs are connected to the power grid without any control or coordination over when and how they charge. In this mode, EVs are simply plugged in, and the charging process begins immediately at the maximum charging rate supported by the vehicle and the charging infrastructure. The outcome of such an arrangement can be seen in Figure 5. The figure shows the EV charging current I_{EV}, which is the current taken by the charging station buck converter, which varies with respect to time. A variable step EV charging current is taken to realize the random plug-in and out-of vehicles. The load voltage, although mentioned V_{CL} to keep on the context of the study, actually resembles the load voltage. Without any control algorithm and/or DSM with the variation of the charging current, the system power demand varies, changing the system voltage. It can be clearly seen that the system voltage reduces from 217 to 195 V, with the charging current varying from 0 to 62 A. The buck converter maintains the output voltage at 48 V throughout the operation, which can be seen in Figure 5. In uncontrolled charging, there is no communication or coordination between the EVs and the grid, meaning that EVs start charging whenever they are connected, irrespective of the grid's load conditions or electricity prices. Hence, required measures need to be taken.

5.2. Rapid Transition Charge Control. The isolated system becomes vulnerable when EV is introduced in the system due to limitations in source power. When the EV is plugged in there is a drop in load voltage. ES tries to maintain voltage across CL by managing NCL voltage. With the appropriate control approach of the ES, the CL voltage remains constant. CL, NCL, EV voltage, and EV current are displayed in Figure 6(a). So far, it is clear that maintaining the critical voltage at a fixed nominal value is done through the coordinated action of ES and NCL. Since NCL voltage is decreased/increased whenever an additional load gets connected/disconnected. From the real-time simulation results, the subsequent voltage drop/rise in NCL is considered to be an event of EV connection/disconnection.

In the proposed work, CL consists of a linear RL load and an EV charging station. The EV charging station consists of a rectifier and charge controller, which reduces the charging voltage to a range of 52–48 V for the purpose of battery charging. In this subsection, the EVs are charged with a fast-charging scheme, where priority is given toward minimizing the charging time of the vehicle. The EV charging current is varied in steps, as seen in Figure 6(c). Due to variations in charging current, the CL power varies accordingly, which is evident in Figure 6(b). Charging voltage is maintained at its maximum value of 52 V, as can be seen in

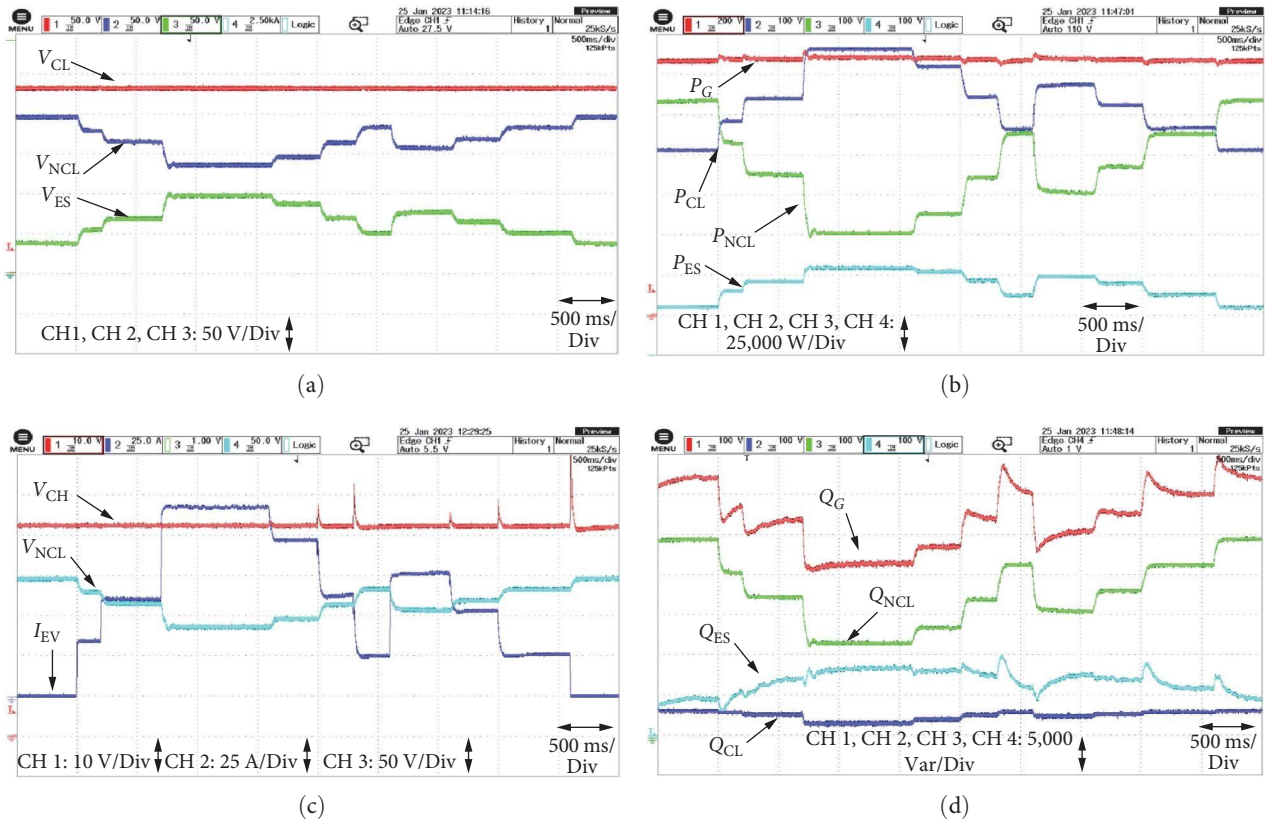

FIGURE 6: Charging of multiple vehicles with RTCC: (a) CL, NCL, and ES voltage; (b) system, CL, NCL, and ES active power; (c) charging voltage, EV current, NCL voltage, and trigger; (d) system, CL, NCL, and ES reactive power.

Figure 6(c). Due to heavy charging currents, the system voltage tends to reduce. The ES senses the CL voltage and suppresses the NCL voltage to maintain a constant voltage profile, which is evident in Figure 6(a). Due to the action of the ES, the NCL voltage drops to 132 V at its minimum, as shown in Figure 6(a). This drop in voltage causes the NCL active and reactive power to drop, as can be seen in Figures 6(b) and 6(d). As the charging voltage is kept at a constant voltage, priority is given to vehicle charging time, whereas the NCL voltage profile gets deteriorated, which is quite undesirable in aspects of consumer standards.

5.3. Smoothing Band Charge Control (SBCC). In this second charging scheme, the Authors have proposed a novel charging structure that can switch itself between fast and slow charging when needed. In this charging scheme, priority is given to voltage profiling of the NCL. The charging scheme switches between fast and slow charging depending on the NCL voltage profile.

Assuming an operating range of NCL voltage between 0.65 and 1.2 p.u., the limit is set at 150 V, below which slow charging is enabled. This particular voltage is named as fast charging threshold (FCT). Since the allowable voltage variation for low voltage circuits is ±10%, which is found to be ±23 V for FCT. Hence, the smoothing band voltage is set at 20 V. Here, the same EV current profile is used as in the previous case, which can be seen in Figure 7(c). In the previous case, the NCL voltage falls to 132 V. During the time duration of t_1 and t_2, the trigger is enabled. Due to that, the charging scheme is switched from fast charging to slow charging. As the switching scheme changes, the charging voltage is reduced from 52 to 48.6 V, as can be seen in Figure 7(c). The reduction in charging voltage reduces the charging current as compared to the previous case. The difference in charging currents of the two cases can be seen in Figure 8(c). This reduction in charging current results in suppressed CL active and reactive power during time span t_1 and t_2, which can be noticed in Figures 8(b) and 8(d). This reduction in CL power leaves more room for the NCL. Thus, the NCL voltage is improved, and the NCL also consumes more power as compared to the previous case within time t_1 to t_2. The improvement in NCL voltage can be noticed in Figure 8(a). The increase in NCL active and reactive power can be seen in Figures 8(b) and 8(d), respectively. The comparative active and reactive power injected by the ES can also be viewed in Figure 8(d).

5.4. FFT Analysis. As the EV charging station consists of a rectifier load, which is nonlinear in nature, it injects harmonics in the CL currents. The FFT of the charging station AC side charging current is shown in Figure 9(b). The harmonic orders and THD of the EV charging currents are given in Table 2. It is seen that the EV charging current has a THD of 31.12%, which is quite high. But the CL load current has a lesser THD as compared to the EV current, which is due to the linear nature of the rest of the CL excepting EV charging

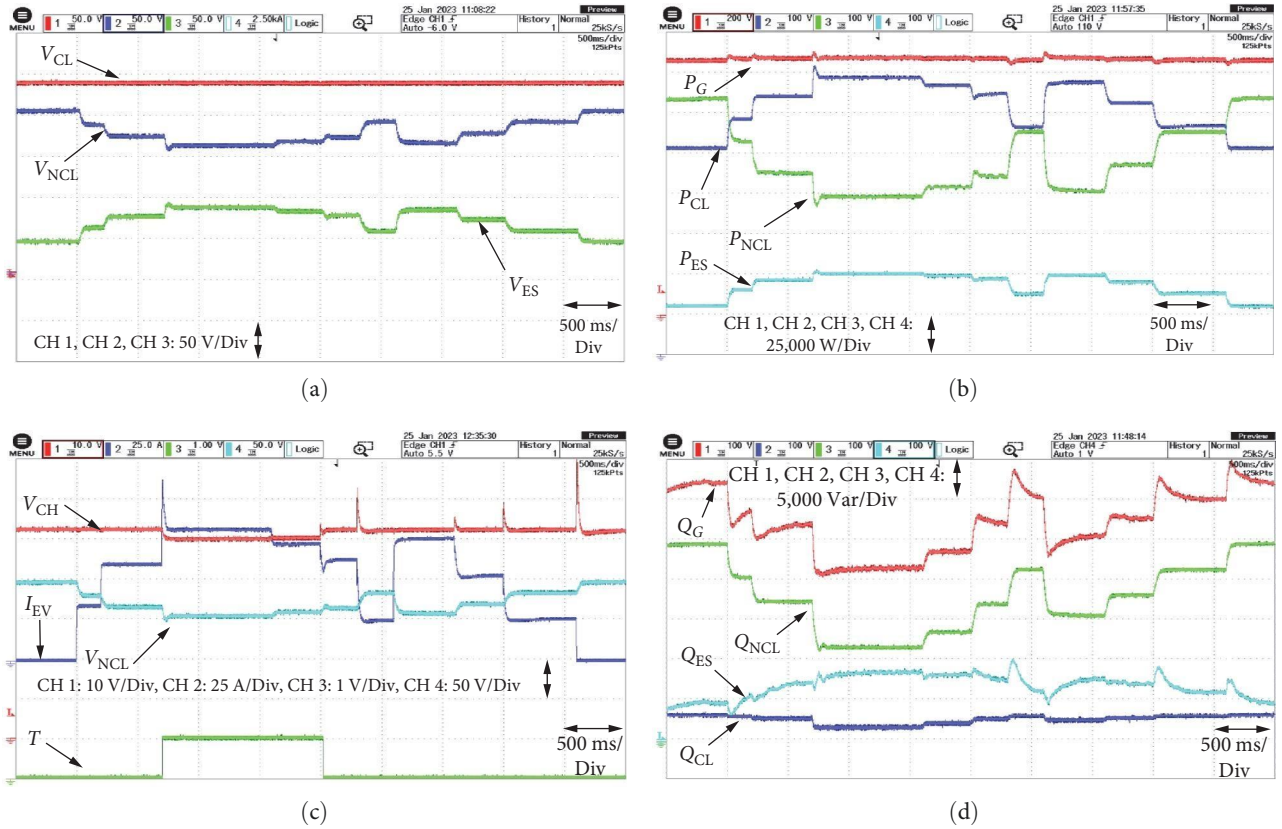

FIGURE 7: Charging of multiple vehicles with SBCC: (a) CL, NCL, and ES voltage; (b) system, CL, NCL, and ES active power; (c) charging voltage, EV current, NCL voltage, and trigger; (d) system, CL, NCL, and ES reactive power.

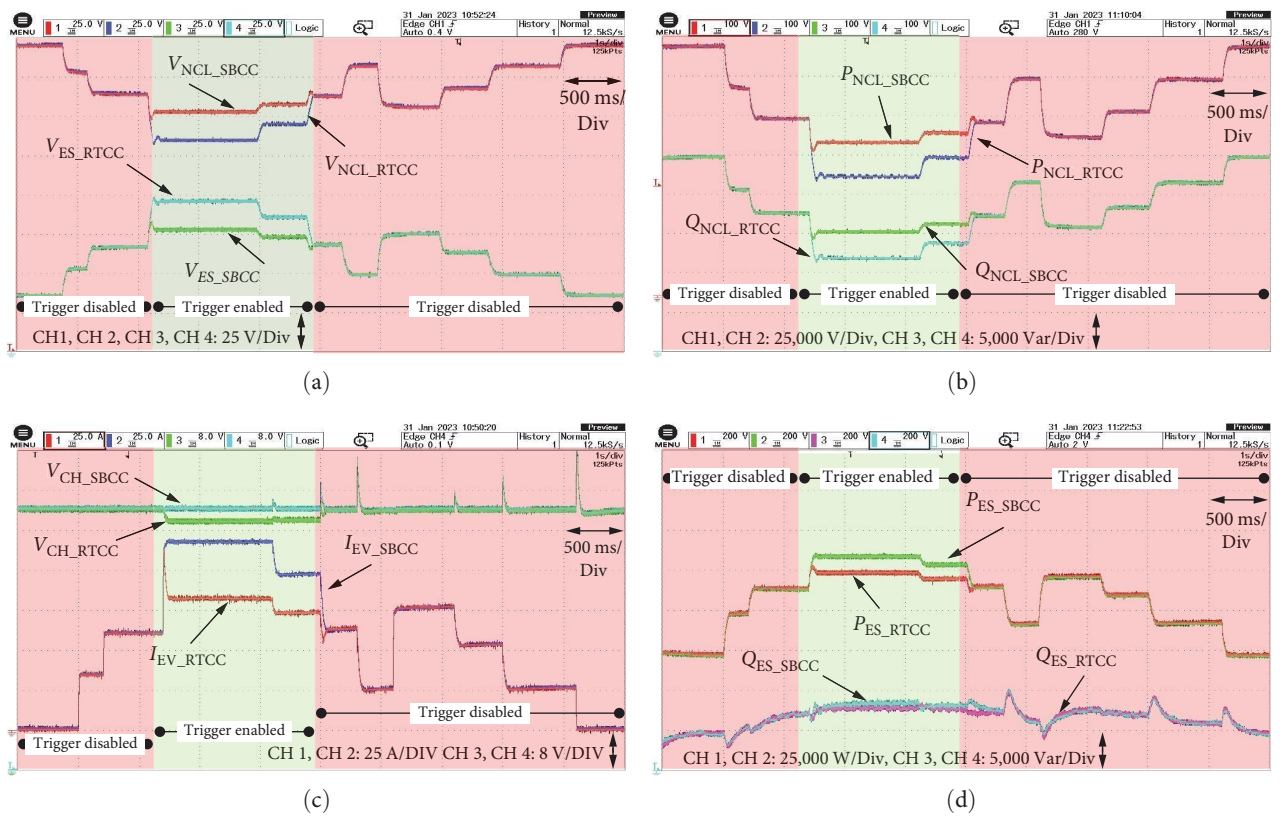

FIGURE 8: Comparison of RTCC and SBCC: (a) NCL voltage and ES voltage; (b) NCL active power and NCL reactive power; (c) charging voltage and EV current; (d) ES active power and ES reactive power.

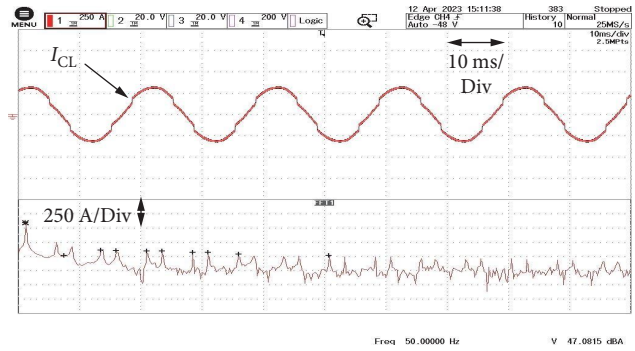

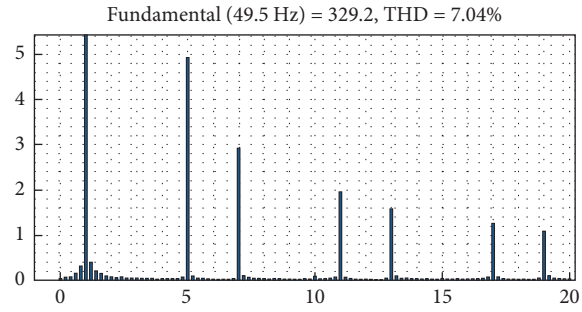

(a)

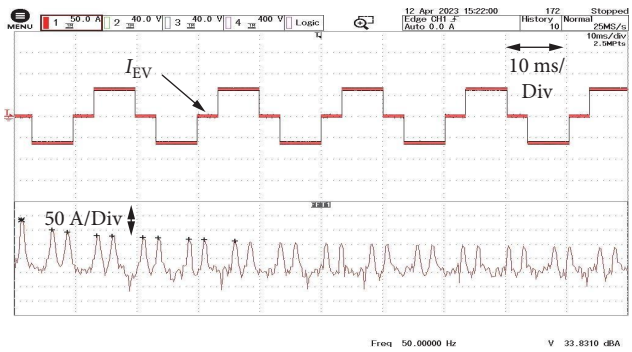

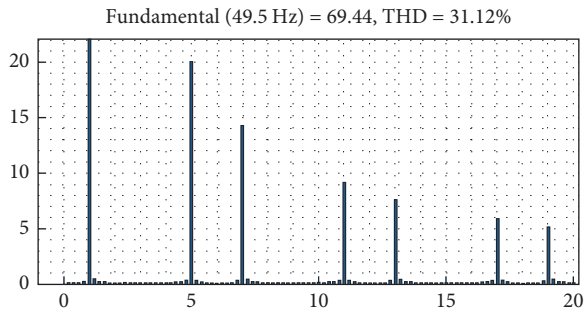

(b)

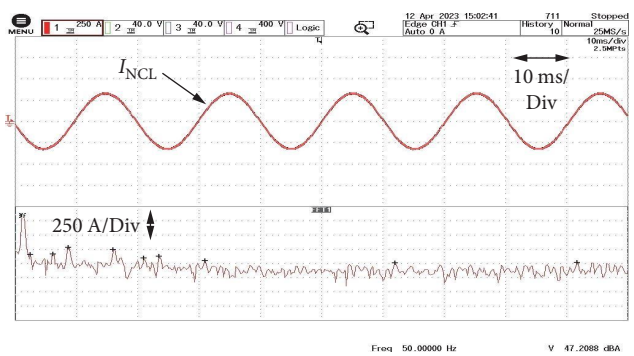

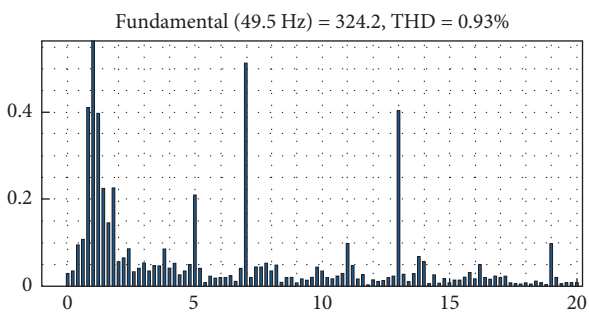

(c)

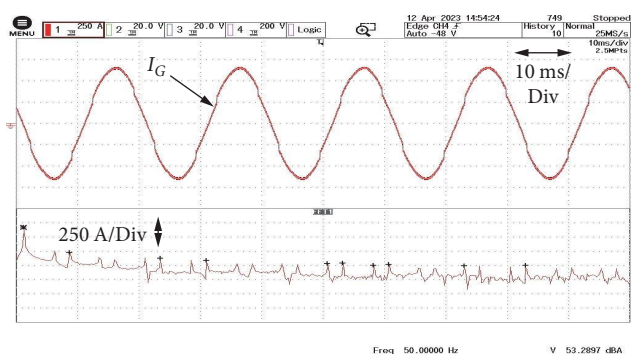

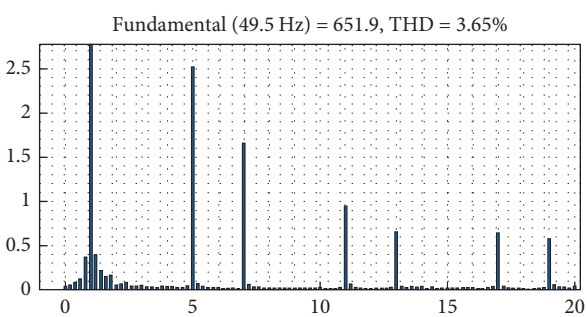

(d)

Figure 9: Continued.

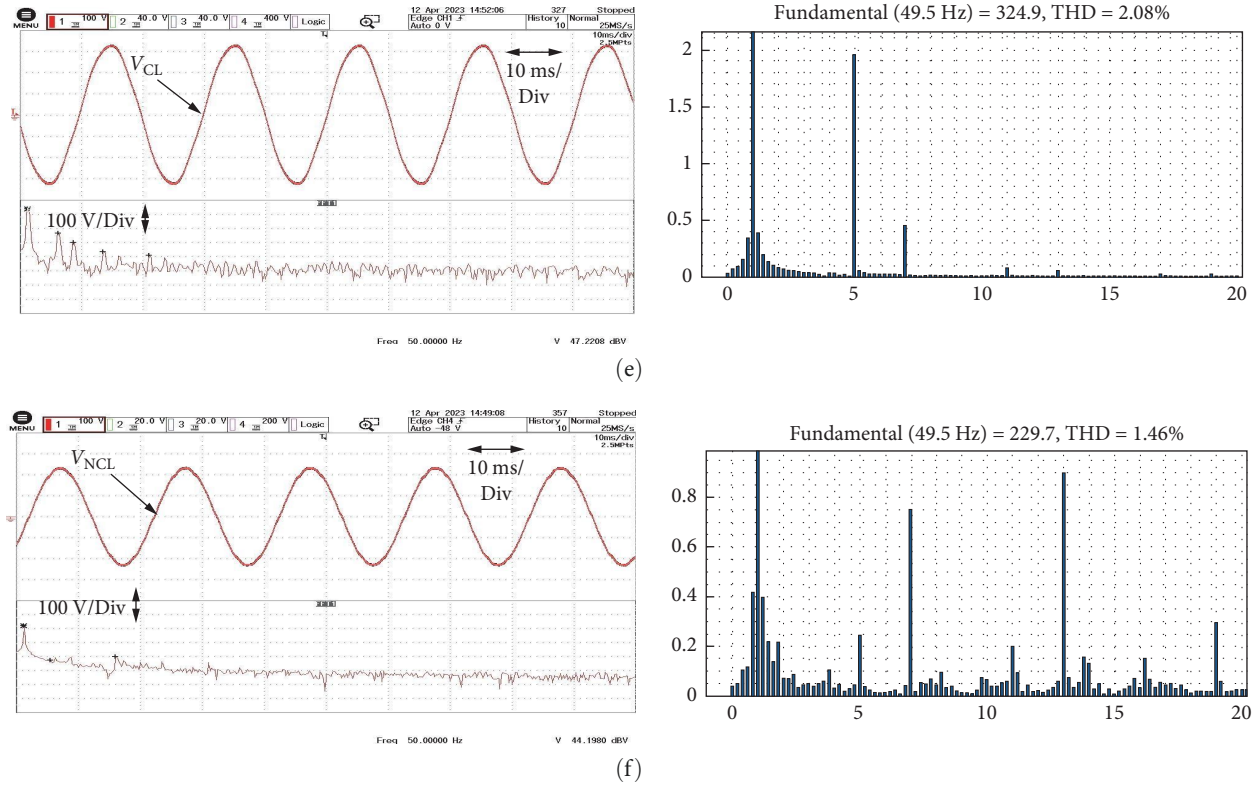

Figure 9: Real-time FFT and THD analysis of (a) CL current, (b) EV current, (c) NCL current, (d) system current, (e) CL voltage, and (f) NCL voltage waveforms.

Table 2: FFT and THD analysis of different current and voltage signal.

THD	I_{CL} 7.04%	I_{EV} 31.12%	I_{NCL} 0.93%	I_G 3.65%	V_{CL} 2.08%	V_{NCL} 1.46%
Harmonic orders	Values in dB					
Fundamental (50 Hz)	47.29	33.96	47.2	53.27	47.22	44.18
2nd			−7.9			
4th						−5.13
5th	20.26	19.32	−7	17.5	12.9	
7th	18.4	16.34	2.48		−0.28	
11th	9.3	11.62			−13.5	
13th	9.12	10.65	−1.09			−0.157
17th	8.6	8.95	−12.85		−18.7	
19th	8.16	8.19		9.6		
23rd	6.83	6.55				
25th	5.93	5.77	−10.46	6.8		
29th	3.4	3.95				
41st				2.42		
43rd				2.58		
47th				−0.22		
49th			−16.26	1.19		

station. Apart from the charging station, the ES also injects some number of harmonics in the system voltage. In this work, the FFT analysis of the various voltages is also done, and the results are given in Figures 9(e) and 9(f), respectively. It can be seen that the system voltage or the voltage across CL is not purely sinusoidal due to the presence of the EV charging station. The CL voltage has a THD of 2.08%, which can be seen in Figure 9(e). But on contrary, the NCL voltage has a nearly sinusoidal waveform, which is evident in Figure 9(f). This is due to the fact that the ES acts as an active

Table 3: Comparison with other competitive charging approaches.

Reported research	Charging technology	Grid type	Voltage regulation	Remarks
Crozier et al. [10]	Uncontrolled	Grid connected	Load dependent (degrades with loading)	Customer-supportive
Clairand et al. [13]	Source capacity dependent	Isolated	EV aggregator dependent	System-supportive
Shaaban et al. [12]	Cost controlled	Distribution grid	Regulated only below the planned charging capacity	Both customer-supportive and system-supportive
Wang et al. [14]	Coordinated charging	Distribution grid	subjected to complex power flow control	Customer-supportive
Proposed	Controlled	Isolated	Due to "smart load + smoothening band charging"	Both customer-supportive and system-supportive

voltage filter and filters out the harmonics from the NCL voltage. This is why the NCL voltage becomes sinusoidal. From Table 2, it can be clearly noticed that the EV charging station injects mostly the odd harmonics into the system current. These harmonics propagate in the system and also appear in the CL voltage. But due to the voltage filtering action of the ES, these harmonics are mostly filtered out on the NCL side. Only some very higher order harmonics of the order 43rd, 56th, and 58th are present in the NCL voltage and currents, which are very less in amplitude. The higher order harmonics appear as a result of the switching of the ES. From Figure 9 and Table 2, it can be seen that despite having nonlinear elements in the system the system, voltage and currents possess harmonics within allowable limits.

5.5. Comparative Review. A comparative study is conducted with other prepublished EV charging approaches, as stated in Table 3. The most common one is uncontrolled charging, where the EVs are allowed to be charged with maximum rating, leading to poor voltage regulation, as explained in the study of Crozier et al. [10]. If the charging depends solely upon source capacity, then there might be cases where RES displays uncertainty, due to which the entire system is affected [13]. The cost control mechanism is suggested in the study of Shaaban et al. [12] only limited to small communities, and voltage regulation is going to be increasingly difficult with respected to installed capacity. Further coordinated control [14] can be scalable, but regulation is highly dependent on proper power flow control. On the contrary, the proposed band-controlled charging mechanism simply operates the charging speed in a smoother way with a simple SL approach. Here, the most prominent advantage is the voltage remains unaffected while increasing the load on the charging station subjected to conciliation in the speed of charging.

6. Conclusion

This article introduces a novel EV charging control strategy designed for a remote islanded area where RES is the only feasible source of energy. A wind energy-based SEIG along with ES SL concept are used to study the sustainability of the system in the worst possible scenario. The article has aimed at enhancing the NCL voltage profile up to a certain extent by imposing the proposed EV control strategy, named the "smoothing band charge control." SBCC can intelligently switch between fast and slow-charging methods to improve the NCL voltage. When the NCL voltage drops below 150 V, the system employs the slow charging method, and when it rises above 170 V, it activates the fast-charging method. The transition between these charging methods is made smooth by introducing a voltage band of 20 V in the switching algorithm. Through result analysis, it was observed that the proposed control strategy can enhance the NCL voltage by nearly 23 V, based on the same EV loading profile. In addition to the NCL voltage improvement, the ES also contributes to enhancing power quality on the NCL side. It effectively filters out the harmonics generated by the EV charging station, thereby improving the voltage and current waveforms on the NCL side. Overall, the suggested control structure is found to be effective in improving the voltage profile and power quality on the NCL side. Additionally, the ES successfully maintains a stable voltage profile on the conventional load (CL) side. The article further compares the results of the proposed approach with other competitive methods and finds that it offers superior voltage regulation without the need for complex control methods. This makes the proposed control strategy a practical and efficient solution for enhancing EV charging and voltage stability in isolated systems with energy storage integration.

Data Availability

The data that support the findings of this study are available from the corresponding author upon reasonable request.

Conflicts of Interest

The authors declare that they have no conflicts of interest.

References

[1] Y. Kuang, Y. Zhang, B. Zhou et al., "A review of renewable energy utilization in islands," *Renewable and Sustainable Energy Reviews*, vol. 59, pp. 504–513, 2016.

[2] S. Djørup, J. Z. Thellufsen, and P. Sorknæs, "The electricity market in a renewable energy system," *Energy*, vol. 162, pp. 148–157, 2018.

[3] X. Sun, Z. Li, X. Wang, and C. Li, "Technology development of electric vehicles: a review," *Energies*, vol. 13, no. 1, Article ID 90, 2020.

[4] M. Saritha and P. V. Manitha, "Power quality issues on the integration of RES-EV to grid: a review," in *2022 International Conference on Innovations in Science and Technology for Sustainable Development (ICISTSD)*, pp. 347–352, IEEE, Kollam, India, 2022.

[5] X. Zhu, M. Xia, and H.-D. Chiang, "Coordinated sectional droop charging control for EV aggregator enhancing frequency stability of microgrid with high penetration of renewable energy sources," *Applied Energy*, vol. 210, pp. 936–943, 2018.

[6] K. Y. Yap, C. R. Sarimuthu, and J. M.-Y. Lim, "Virtual inertia-based inverters for mitigating frequency instability in grid-connected renewable energy system: a review," *Applied Sciences*, vol. 9, no. 24, Article ID 5300, 2019.

[7] A. Khan, S. Memon, and T. P. Sattar, "Analyzing integrated renewable energy and smart-grid systems to improve voltage quality and harmonic distortion losses at electric-vehicle charging stations," *IEEE Access*, vol. 6, pp. 26404–26415, 2018.

[8] A. K. Karmaker, S. Roy, and M. R. Ahmed, "Analysis of the impact of electric vehicle charging station on power quality issues," in *2019 International Conference on Electrical, Computer and Communication Engineering (ECCE)*, pp. 1–6, IEEE, Cox'sBazar, Bangladesh, 2019.

[9] M. Nour, J. P. Chaves-Ávila, G. Magdy, and Á. Sánchez-Miralles, "Review of positive and negative impacts of electric vehicles charging on electric power systems," *Energies*, vol. 13, no. 18, Article ID 4675, 2020.

[10] C. Crozier, T. Morstyn, and M. McCulloch, "The opportunity for smart charging to mitigate the impact of electric vehicles on transmission and distribution systems," *Applied Energy*, vol. 268, Article ID 114973, 2020.

[11] S.-G. Yoon and S.-G. Kang, "Economic microgrid planning algorithm with electric vehicle charging demands," *Energies*, vol. 10, no. 10, Article ID 1487, 2017.

[12] M. F. Shaaban, S. Mohamed, M. Ismail, K. A. Qaraqe, and E. Serpedin, "Joint planning of smart EV charging stations and DGs in eco-friendly remote hybrid microgrids," *IEEE Transactions on Smart Grid*, vol. 10, no. 5, pp. 5819–5830, 2019.

[13] J.-M. Clairand, J. Rodríguez-García, and C. Álvarez-Bel, "Electric vehicle charging strategy for isolated systems with high penetration of renewable generation," *Energies*, vol. 11, no. 11, Article ID 3188, 2018.

[14] J. Wang, G. R. Bharati, S. Paudyal, O. Ceylan, B. P. Bhattarai, and K. S. Myers, "Coordinated electric vehicle charging with reactive power support to distribution grids," *IEEE Transactions on Industrial Informatics*, vol. 15, no. 1, pp. 54–63, 2019.

[15] A. Ahmad, A. Ullah, C. Feng et al., "Towards an improved energy efficient and end-to-end secure protocol for iot healthcare applications," *Security and Communication Networks*, vol. 2020, Article ID 8867792, 10 pages, 2020.

[16] S. Ashraf, O. Alfandi, A. Ahmad et al., "Bodacious-instance coverage mechanism for wireless sensor network," *Wireless Communications and Mobile Computing*, vol. 2020, Article ID 8833767, 11 pages, 2020.

[17] S. Ashraf, T. Ahmed, Z. Aslam, D. Muhammad, A. Yahya, and M. Shuaeeb, "Depuration based efficient coverage mechanism for wireless sensor network," *Journal of Electrical and Computer Engineering Innovations (JECEI)*, vol. 8, no. 2, pp. 145–160, 2020.

[18] M. Zhang and J. Chen, "The energy management and optimized operation of electric vehicles based on microgrid," *IEEE Transactions on Power Delivery*, vol. 29, no. 3, pp. 1427–1435, 2014.

[19] S. G. Liasi and S. M. T. Bathaee, "Optimizing microgrid using demand response and electric vehicles connection to microgrid," in *2017 Smart Grid Conference (SGC)*, pp. 1–7, IEEE, Tehran, Iran, 2017.

[20] S. G. Liasi and M. A. Golkar, "Electric vehicles connection to microgrid effects on peak demand with and without demand response," in *2017 Iranian Conference on Electrical Engineering (ICEE)*, pp. 1272–1277, IEEE, Tehran, Iran, 2017.

[21] S. Liu, J. Jiang, and G. Cheng, "Research on vector control strategy of three phase VIENNA rectifier employed in EV charger," in *2019 Chinese Control and Decision Conference (CCDC)*, pp. 4914–4917, IEEE, Nanchang, China, 2019.

[22] Xi Zhang and Z. Zheng, "Application of repetitive control in electric spring," *IEEE Access*, vol. 8, pp. 216607–216616, 2020.

[23] S. Acharya, M. S. El-Moursi, A. Al-Hinai, A. S. Al-Sumaiti, and H. H. Zeineldin, "A control strategy for voltage unbalance mitigation in an islanded microgrid considering demand side management capability," *IEEE Transactions on Smart Grid*, vol. 10, no. 3, pp. 2558–2568, 2019.

[24] T. Chen, H. Liu, C.-K. Lee, and S. Y. R. Hui, "A generalized controller for electric-spring-based smart load with both active and reactive power compensation," *IEEE Journal of Emerging and Selected Topics in Power Electronics*, vol. 8, no. 2, pp. 1454–1465, 2020.

[25] J. Chen, S. Yan, T. Yang, S.-C. Tan, and S. Y. Hui, "Practical evaluation of droop and consensus control of distributed electric springs for both voltage and frequency regulation in microgrid," *IEEE Transactions on Power Electronics*, vol. 34, no. 7, pp. 6947–6959, 2019.

[26] S. Mohanty, S. Pati, and S. K. Kar, "Persistent voltage profiling of a wind energy-driven islanded microgrid with novel neuro-fuzzy controlled electric spring," *Journal of Control, Automation and Electrical Systems*, vol. 34, pp. 609–623, 2023.

[27] A. Kaymanesh and A. Chandra, "Electric spring using MPUC5 inverter for mitigating harmonics and voltage fluctuations," *IEEE Journal of Emerging and Selected Topics in Power Electronics*, vol. 9, no. 6, pp. 7447–7458, 2021.

[28] Z. Zhang, C. Xie, R. Tong, and S. Gao, "Identification and control of electric elasticity limit for electric-spring-based flexible loads," *IEEE Transactions on Industrial Informatics*, vol. 15, no. 11, pp. 6001–6010, 2019.

[29] S. Yan, C.-K. Lee, T. Yang et al., "Extending the operating range of electric spring using back-to-back converter: hardware implementation and control," *IEEE Transactions on Power Electronics*, vol. 32, no. 7, pp. 5171–5179, 2017.

[30] R. Pawar, S. P. Gawande, S. G. Kadwane, M. A. Waghmare, and R. N. Nagpure, "Five-level diode clamped multilevel inverter (DCMLI) based electric spring for smart grid applications," *Energy Procedia*, vol. 117, pp. 862–869, 2017.

[31] L. Liang, Y. Hou, and D. J. Hill, "Enhancing flexibility of an islanded microgrid with electric springs," *IEEE Transactions on Smart Grid*, vol. 10, no. 1, pp. 899–909, 2019.

[32] C. K. Lee, B. Chaudhuri, and S. Y. Hui, "Hardware and control implementation of electric springs for stabilizing future smart grid with intermittent renewable energy sources," *IEEE Journal of Emerging and Selected Topics in Power Electronics*, vol. 1, no. 1, pp. 18–27, 2013.

[33] S.-C. Tan, C. K. Lee, and S. Y. Hui, "General steady-state analysis and control principle of electric springs with active

and reactive power compensations," *IEEE Transactions on Power Electronics*, vol. 28, no. 8, pp. 3958–3969, 2013.

[34] T. Yang, K.-T. Mok, S.-C. Tan, C. K. Lee, and S. Y. Hui, "Electric springs with coordinated battery management for reducing voltage and frequency fluctuations in microgrids," *IEEE Transactions on Smart Grid*, vol. 9, no. 3, pp. 1943–1952, 2018.

[35] S. Yan, C.-K. Lee, T. Yang et al., "Extending the operating range of electric spring using back-to-back converter: hardware implementation and control," *IEEE Transactions on Power Electronics*, vol. 32, no. 7, pp. 5171–5179, 2017.

[36] M.-H. Wang, S.-C. Tan, C.-K. Lee, and S. Y. Hui, "A configuration of storage system for DC microgrids," *IEEE Transactions on Power Electronics*, vol. 33, no. 5, pp. 3722–3733, 2018.

[37] T. Yang, K.-T. Mok, S.-S. Ho, S.-C. Tan, C.-K. Lee, and R. S. Y. Hui, "Use of integrated photovoltaic-electric spring system as a power balancer in power distribution networks," *IEEE Transactions on Power Electronics*, vol. 34, no. 6, pp. 5312–5324, 2019.

[38] M. Norouzi, J. Aghaei, S. Pirouzi, T. Niknam, and M. Lehtonen, "Flexible operation of grid-connected microgrid using ES," *IET Generation, Transmission & Distribution*, vol. 14, no. 2, pp. 254–264, 2020.

[39] M.-H. Wang, T.-B. Yang, S.-C. Tan, and S. Y. Hui, "Hybrid electric springs for grid-tied power control and storage reduction in AC microgrids," *IEEE Transactions on Power Electronics*, vol. 34, no. 4, pp. 3214–3225, 2019.

[40] R. S. Pawar, S. P. Gawande, R. N. Nagpure, and M. A. Waghmare, "Modified instantaneous symmetrical component algorithm-based control for operating electric spring in active power filter mode," *IET Power Electronics*, vol. 12, no. 7, pp. 1730–1741, 2019.

[41] Ankita and R. K. Jarial, "Improved electric spring control for power factor correction using fuzzy PI controller," in *2022 2nd International Conference on Emerging Frontiers in Electrical and Electronic Technologies (ICEFEET)*, pp. 1–6, IEEE, Patna, India, 2022.

[42] M. S. Javaid, A. Sabir, M. A. Abido, and H. R. E. H. Bouchekara, "Electric spring controller design for distribution network loaded by electric vehicles," *IET Energy Systems Integration*, vol. 1, no. 4, pp. 246–251, 2019.

[43] M. Norouzi, J. Aghaei, S. Pirouzi, T. Niknam, M. Fotuhi-Firuzabad, and M. Shafie-khah, "Hybrid stochastic/robust flexible and reliable scheduling of secure networked microgrids with electric springs and electric vehicles," *Applied Energy*, vol. 300, Article ID 117395, 2021.

[44] B. Singh, S. S. Murthy, and S. Gupta, "Analysis and design of STATCOM-based voltage regulator for self-excited induction generators," *IEEE Transactions on Energy Conversion*, vol. 19, no. 4, pp. 783–790, 2004.

[45] H. Kim, J.-H. Kim, and S.-K. Sul, "A design consideration of output filters for dynamic voltage restorers," in *2004 IEEE 35th Annual Power Electronics Specialists Conference (IEEE Cat. No. 04CH37551)*, pp. 4268–4272, IEEE, Aachen, Germany, 2004.

[46] X. Luo, Z. Akhtar, C. K. Lee, B. Chaudhuri, S.-C. Tan, and S. Y. R. Hui, "Distributed voltage control with electric springs: comparison with STATCOM," *IEEE Transactions on Smart Grid*, vol. 6, no. 1, pp. 209–219, 2015.